Received: 22 April 2025 | Revised: 29 August 2025 | Accepted: 29 September 2025

DOI: 10.1111/jace.70317

Journal of the American Ceramic Society

RESEARCH ARTICLE

Chemical strengthening of float glasses: Effect of composition and structure

Vincenzo M. Sglavo[1,2] | **Paolo Bettotti**[3] | **Emanuela Callone**[1,4] | **Sandra Dirè**[1,4]

This paper is dedicated to the memory of Prof. David J. Green (The Pennsylvania State University), mentor of Vincenzo M. Sglavo, a great instructor and scientist.

[1]Dipartimento di Ingegneria Industriale, Università degli Studi di Trento, Trento, Italy

[2]Istituto di Fotonica e Nanotecnologie, Consiglio Nazionale delle Ricerche, Trento, Italy

[3]Dipartimento di Fisica, Università degli Studi di Trento, Trento, Italy

[4]"Klaus Müller" Magnetic Resonance Laboratory, Dipartimento di Ingegneria Industriale, Università sdegli Studi di Trento, Trento, Italy

Correspondence
Vincenzo M. Sglavo and Emanuela Callone, Dipartimento di Ingegneria Industriale, Università degli Studi di Trento, Via Sommarive 9, I-38123 Trento, Italy.
Email: vincenzo.sglavo@unitn.it and emanuela.callone@unitn.it

Abstract

Two silicate float glasses were considered in the present work: a typical clear soda lime silicate glass and a soda magnesia silicate glass. Both materials underwent chemical strengthening in KNO_3, and a different behavior was pointed out in terms of potassium penetration and corresponding surface compression. The soda magnesia silicate glass demonstrated a significantly higher propensity for reinforcement through the exchange of sodium with potassium owing to a much higher interdiffusion coefficient, although the activation energy for the process was substantially identical for the two materials. The difference in performance in terms of Na/K exchange can be only partially correlated to the slightly larger amount of sodium in the soda-magnesia silicate glass, which is instead characterized by a more open structure, richer in five-, six-membered or larger rings, as revealed by NMR and FT-IR/micro-Raman spectroscopy. This structural difference appears to be dictated by the chemical composition of the glasses, soda magnesia silicate material being richer in network formers such as silica, alumina, and, very likely, magnesia, which causes the presence of more abundant Q^3 units and more limited Q^2 and Q^4 ones for a faster movement of the alkaline atoms within the structure.

KEYWORDS

chemical strengthening, FT-IR spectroscopy, glass structure, ion exchange, Raman spectroscopy, silicate glass, solid state NMR

1 | INTRODUCTION

Chemical strengthening is nowadays widely used to reinforce silicate glass articles with a multitude of applications from personal electronic devices to pharmaceutical packaging and autoinjectors, from kitchenware articles to optical devices, from armor components to windows in buildings or windshields in airplanes, ships, or cars. It was introduced exactly sixty years ago by Acloque and Tochon.[1] It is based on an ion exchange process carried out at temperatures below T_g, where smaller alkaline ions (typically Li or Na) in the glass are substituted by larger ones (Na or K), typically present in a salt in contact with the glass itself. This creates a "stuffing" effect in the glass

surface structure, which generates a residual compression, useful to shield surface flaws and improve the tensile or bending resistance, or to make the creation of additional defects more difficult.[2–5] At the industrial level, the process is typically performed by immersing the glass articles, collected in a stainless-steel basket, in a molten salt (usually KNO_3 or $NaNO_3$) for several hours, taking them out, and washing with water. With respect to other glass-reinforcing techniques (above all, thermal tempering), chemical strengthening has the advantage of being applied to articles with highly variable shapes and thicknesses, with no optical distortions, and to generate very intense surface compression. On the other side, the process is usually very long (in the order of some hours) and the glass thickness under compression is normally relatively thin, very often below 50 μm.

Several strategies have been advanced to improve the chemical strengthening efficiency, for example, by using glasses with higher transition temperature or containing lithium ions, to make the interdiffusion faster, although avoiding the relaxation of the generated stresses, or using external electrical fields or ultrasounds to make the ion exchange faster.[3] The improvement of the glass composition to make it prone to be chemically strengthened by ion exchange represents a suitable path for a technology even more affordable, less expensive, and more widespread. Some indications have been reported, for example, in a review by Varshneya,[3] who stated that the use of mixed alkali compositions or MgO additions in the glass can have beneficial effects for common-use silicate glasses, used for containers, plates, or windows. Nevertheless, the research on this matter is still not plentiful. One limitation surely relies on the fact that most of the glass articles are produced by soda lime silicate glass, and there is not much room for modifications to the composition due to the existing plants, industrial and technological constraints.

In the present work, two soda lime silicate glasses were compared in terms of their chemical tempering efficiency: a very typical clear float glass and an innovative float material with slightly different composition but very similar thermoelastic properties, with the aim to point out how even small differences can determine a drastic alteration once subjected to identical ion exchange processes, thus giving indications for possible future modification of glass compositions properly tailored for being chemically strengthened more efficiently.

2 | MATERIALS AND METHODS

Two silicate float glasses were considered in the present work: a typical 4 mm-thick clear soda lime silicate glass (SLS) and a soda magnesia silicate glass (Glanova) from Pilkington Italia Spa—NSG group with a thickness of 1 mm (SMS). The two glasses are labelled as SLS and SMS in the following. Chemical composition, density, elastic moduli, and transition temperature of the glasses are shown in Table 1. The composition was determined by X-ray fluorescence; the density was measured by Archimedes' method; Young's and shear modulus were determined by acoustic resonance method (ASTM C623 norm); the T_g was evaluated by differential scanning calorimetry.

TABLE 1 Composition, density, Young's and shear modulus, T_g, and refractive index of the glasses used in the present work.

	Soda lime silicate glass		Soda magnesia silicate glass	
	wt%	mol%	wt%	mol%
SiO_2	71.8	70.7	68.7	67.6
Na_2O	12.8	12.6	15.4	14.7
MgO	3.6	5.3	8.8	12.9
Al_2O_3	1.4	0.8	4.8	2.8
CaO	9.5	10.0	1.7	1.8
K_2O	0.9	0.6	0.3	0.2
Density (g/cm^3)	2.51 ± 0.01		2.45 ± 0.01	
Young's modulus (GPa)	72 ± 1		72 ± 1	
Shear modulus (GPa)	30 ± 2		31 ± 2	
T_g (°C)	582 ± 3		589 ± 3	
Refractive index @ 543.5 and 632.8 nm	1.525/1.521		1.512/1.510	

The glass sheets were cut into 3 × 3 cm^2 samples whose edges were polished using 800 grit silicon carbide abrasive paper. Air and tin sides of the glasses were identified by exposing them to shortwave UV light because in these conditions only the tin side glows.

The glass specimens were subjected to various chemical tempering treatments: two durations of 4 and 16 h, and temperatures ranging from 400 to 475°C. Prior to the treatment, all samples were cleaned with ethanol and thoroughly dried. The ion exchange process was carried out by placing each glass sample, one at a time, into stainless steel crucibles containing potassium nitrate salt (Fluka, 99.9%), which had been preheated in a muffle furnace for approximately 1 h to ensure complete melting. After completing the tempering cycle, the samples were carefully removed from the crucible, rinsed with distilled water, and gently dried with soft paper.

Biaxial compressive stress (CS) and depth of compression layer (DOL) were measured on the air side by a surface stress meter (FSM-60LE, Luceo Co, Ltd.) according to the ASTM C1422 standard. A photoelastic constant equal to 2.72 TPa^{-1} was used for the calculations.

The concentration of sodium and potassium on the "air" surface of the chemically tempered glasses was determined by standardless quantitative EDXS (energy dispersion

X-ray spectroscopy) (EDS 2000; IXRF system) within the scanning electron microscope (SEM, JSM5500, Jeol) with the ZAF (Z-atomic number, A-X-ray absorption, F-X-ray fluorescence) matrix-correction method. The base glasses were used as a reference to improve the accuracy of the quantitative chemical analysis in terms of sodium and potassium.[6] The analyzed surfaces were preliminarily metallized with a thin layer of Au–Pd to prevent the electrical charging effect. The following conditions were used for the EDXS analysis: voltage = 20 kV, distance = 20 mm, spot size = 38.

The concentration profiles were measured by the EDXS line-scanning technique on the cross-section of manually broken samples, and at least five scans per sample were collected, always referring to the "air" side of the glasses. To compare the individual measurements, the potassium concentration in each spectrum was normalized to the silicon concentration. The concentration profiles were fitted by using a typical complementary error function[5] (Equation 1):

$$C_K\ (x,t) = C_K^s\ \ erfc\left(\frac{x}{2\sqrt{Dt}}\right), \qquad (1)$$

where C_K^s is the normalized potassium concentration on the surface, x the distance from the surface, t the treatment time, and D the inter-diffusion coefficient. Both D and the penetration depth, d, were estimated by the fitting procedure. In particular, the penetration depth, d, was calculated as the distance from the "air" side at which the potassium relative concentration was reduced to 2% of the surface value, as estimated by the fitting procedure.

For the structural analyses, a certain amount of the raw materials was reduced to powder with a particle size lower than 100 μm by hand milling using an agate mortar. A portion of the powder was subjected to ion exchange treatment at 450°C for 120 h to obtain a theoretically fully exchanged glass. The powder was placed into a stainless-steel crucible containing the molten KNO_3 salt. After the treatment, the solidified salt containing the glass powder was placed in distilled water and stirred to dissolve the salt completely; the solution was then filtered with paper (8 μm) to collect the ion-exchanged glass powder.

The powders (raw and ion-exchanged) were analyzed by ^{29}Si solid-state nuclear magnetic resonance (NMR), micro-Raman, and infrared spectroscopy.

Solid-state NMR analyses were carried out with a Bruker 400WB wide-bore instrument equipped with a 4mm CPMAS probe. The samples were packed into 4 mm zirconia rotors, which were spun at 7 kHz under air flow. The spectra were acquired with a single pulse sequence under the following conditions: ^{29}Si frequency = 79.48 MHz, $\pi/4$ pulse length = 2.2 μs, recycle delay = 350 s, 1k scans.

In addition, ^{29}Si spin–lattice relaxation time (T_1) was measured with the saturation recovery pulse sequence.[7] T_1 characterizes the time span for the return of a spin system (i.e., the magnetization, M_τ, represented by the entire peak area of the spectrum) to its equilibrium along the applied magnetic field after the perturbation produced by the RF pulse. T_1 values were calculated by fitting the area values of the silicon peak as a function of the repetition time (being τ, the interval between two $\pi/2$ pulses) with the exponential saturation function. In case of inhomogeneity or different crystalline domains, multiple exponentials are necessary. In the present case, a good fitting of the M_τ curves was obtained with a double exponential[7] (Equation 2):

$$M_\tau = M_a\ \left[1 - e^{-\tau/T_{1a}}\right] + M_b\left[1 - e^{-\tau/T_{1b}}\right], \qquad (2)$$

where M_a and M_b are the maximum magnetization values of the generic a and b components, respectively, and T_{1a} and T_{1b} the corresponding time constants.[7]

Octakis(trimethylsiloxy)silsesquioxane (Q_8M_8) was used as an external secondary reference for the peak position calibration. The silicon units are labelled according to the usual notation where Q^n represents the tetrafunctional SiO_4 unit and n is the number of oxo-bridges. Accordingly, throughout the text, the term BO refers to bridging oxygens, while NBO indicates nonbridging oxygens. The line-shape fitting was performed using Gaussian components with Bruker Topspin 3.6 software, and it was considered acceptable at a 95% confidence level.

Fourier-transformed infrared spectra (FT-IR) were collected in transmission mode with 64 scans and 4 cm^{-1} resolution in the 4000–400 cm^{-1} range using a Nicolet Avatar 330 instrument. The line-shape fitting was carried out by the DMFit software[8] and considered acceptable with a confidence level of 95%.

Micro-Raman was performed by the Horiba Jobin-Yvon Aramis instrument, an integrated confocal micro-Raman, using 532 and 633 nm laser lines and a grating with 1200 lines/mm. Multiple spectra were collected on each sample for the sake of more reliable results. The spectra were normalized to the highest peak after 4-point baseline subtraction.[9,10] The line-shape fitting was carried out using Gaussian components with DMFit software,[8] and it was considered acceptable with a confidence level of 95%.

3 | RESULTS

Surface compression (CS) and depth of layer (DOL) as measured by the surface stress-meter in the chemically tempered glasses are shown in Figure 1. A similar dependence of CS and DOL can be observed for both materials as a function of ion exchange temperature and time. As

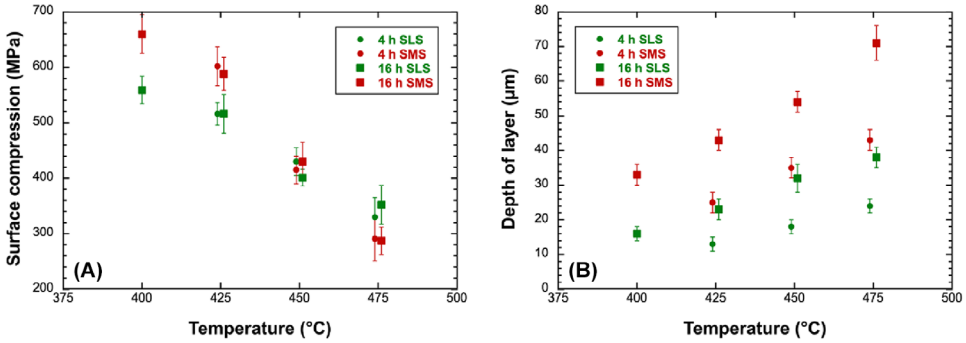

FIGURE 1 Biaxial compressive stress (A), and depth of layer (B), after ion exchange carried out at different temperatures and times. The data points corresponding to 4 h-long treatments are slightly shifted with respect to the actual temperature to avoid overlapping.

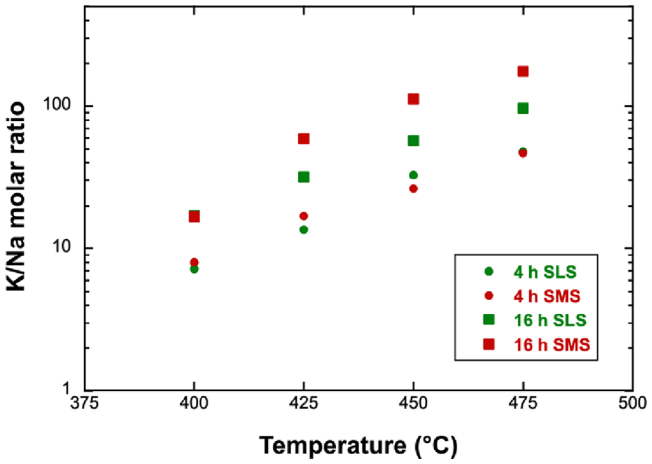

FIGURE 2 K/Na molar ratio measured by EDXS on the surface (air side) of chemically tempered glasses.

expected, the depth of the layer increases with temperature while the surface compression correspondingly reduces, more importantly for SMS glass. Time has a clear effect on DOL only. Very interesting is the intensity of surface compression and, especially, the depth of the layer when comparing the two materials. In SMS glass, the surface compression is always larger, at least for ion exchange temperatures lower than 450°C; more importantly, the depth of the layer is always much larger in the same glass with respect to SLS one under the same processing conditions.

The differences between the two glasses pointed out for "mechanical parameters" like CS and DOL are correlated to some "chemical parameters" strictly dependent on the ion exchange phenomenon at the base of the chemical strengthening process.

Figure 2 shows the K/Na molar ratio on the glasses' surface, as determined by the EDXS analysis at different treatment temperatures. The reported data correspond to the ratio between the moles of potassium and those of sodium on the analyzed surface. To make the reading of the diagram clearer, one has to consider that in the raw glasses the molar ratio is very small (0.05 and 0.01 for SLS and SMS glass, respectively, as from the composition in Table 1); as the ion exchange process proceeds, more and more sodium is substituted on the surface by potassium and this makes the K/Na ratio increasing. It appears that with the shortest exchange time (4 h), a larger amount of sodium is substituted by potassium as the process temperature is increased, in a similar way for both glasses. Instead, for a longer duration (16 h), the exchange between Na and K becomes more and more efficient, especially in SMS glass.

The potassium concentration profiles determined by EDXS line-scan (normalized with respect to the silicon signal to cancel the effect of surface undulations or additional effects which could generate unusual counts) always followed a decreasing trend with respect to the depth and could be easily fitted by using a complementary error function (Equation 1).[5,6] This allowed the calculation of the potassium penetration depth, d, and the interdiffusion coefficient, D, as reported in Figure 3.

For both materials, penetration depth and D increase with temperature, the latter being substantially unaffected by time. Conversely, the potassium penetration strongly depends on the ion exchange duration, the effect being clearly amplified for SMS glass. The difference between the two glasses in terms of Na/K interdiffusion is outstanding; for example, the potassium penetration in SMS glass for every temperature is always larger after 4 h treatment than that achieved after 16 h in SLS glass, this being associated with a greater interdiffusion coefficient.

The data in Figure 3B do follow the typical relationship[2] (Equation 3):

$$\ln D = \ln D_0 - \frac{Q_d}{R\,T}\,, \tag{3}$$

where D_0 is the pre-exponential factor, Q_d the activation energy for diffusion, and R the gas constant. Fitting the data in Figure 3B by Equation (3) allows us to determine the activation energy for diffusion, as reported in Table 2. Despite the quite wide scatter, the values are pretty similar

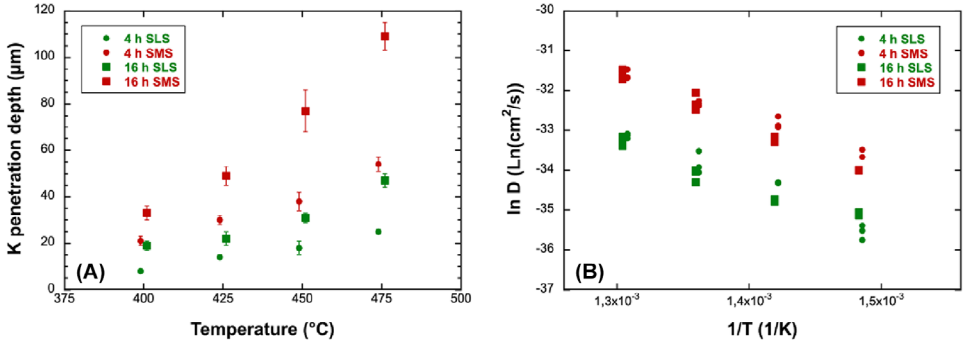

FIGURE 3 Potassium penetration depth (A) and interdiffusion coefficient (B) as estimated by the fitting of the potassium concentration profiles measured by EDXS. The data points in (B) corresponding to 4 h-long treatments are slightly shifted with respect to the actual temperature to avoid overlapping.

TABLE 2 Activation energy for diffusion, Q_d, as determined by fitting the data in Figure 3B.

	Q_d (kJ/mol)	
	4 h	**16 h**
SLS	130 ± 12	101 ± 9
SMS	103 ± 10	135 ± 10

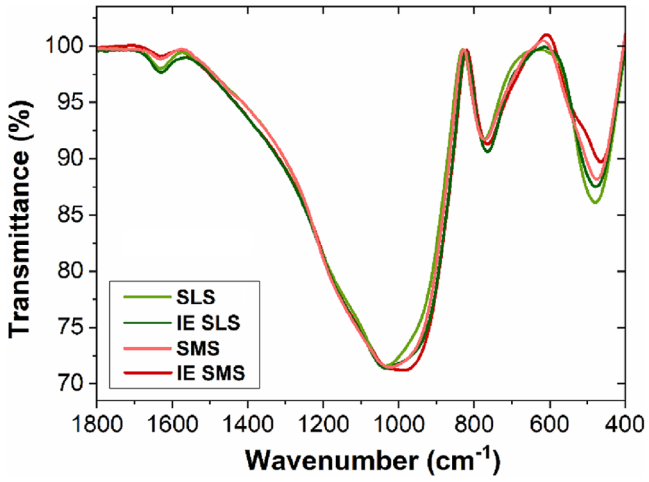

FIGURE 4 FT-IR spectra recorded on raw and ion-exchanged (IE) SLS and SMS glass powders.

for the two glasses, pointing out very similar mechanisms at the basis of the interdiffusion process.

To shed light on these mechanisms at the atomic/molecular level, different spectroscopic techniques were employed, as detailed further in the paper.

Figure 4 shows the FTIR spectra in the 1800–400 cm^{-1} range of interest, recorded on raw and fully tempered SLS and SMS glass powder samples.

The intense band between 1250 and 950 cm^{-1} originates from asymmetric stretching vibrations of Si–O(–Si) bridges (BO) and Si–O^- nonbridging (NBO) bonds in Q^n units. The low-frequency band (400–550 cm^{-1}) is due to the bending mode of Si–O–Si bridges, whereas the symmetric stretching mode is responsible for absorption at 850–700 cm^{-1}.[11–14] The minor peak at 1630 cm^{-1} is associated with water scissoring. The spectra show slight differences among the different samples; in particular, the line shape of the siloxane asymmetric stretching band appears different for the two glasses before and after tempering.

The siloxane asymmetric stretching band can be fitted with four components (Figure S1): the one at about 1120 cm^{-1} is assigned to BO and the components at about 990 and 910 cm^{-1} to NBO, where the component at lower wavenumber is related to species with smaller siloxane angles[13–16]; the broad left shoulder at about 1350 cm^{-1}, which increases after chemical tempering, is still unassigned, although it can be recognized in glass spectra previously reported by some authors.[16]

The raw SMS glass, richer in small ionic radius cations such as Mg^{2+}, has the identified components shifted to lower wavenumbers with respect to the SLS one (Table S1). In addition, both glasses after ion exchange show an increase in the linewidth of low-wavenumber components, whereas the opposite trends are detected for the BO components.[17] The NBO components show a red shift in SLS glass, while a blue shift can be identified by the BO signal in SMS material. The red-shift can be related to the reduction of bond angles[14,18] or to the bond length increase due to the replacement of small cations by larger ones.[17]

The normalized Raman spectra, recorded in the range 200–1400 cm^{-1}, are reported in Figure 5. The spectra exhibit the typical features of soda lime silicate glasses, characterized by three major regions:

(i) The low frequency region (LFR, around 220–700 cm^{-1}), attributed to mixed bending-stretching modes of inter-tetrahedral Si–O–Si bonds[19–21] usually presents different components and provides information about the presence of six or higher

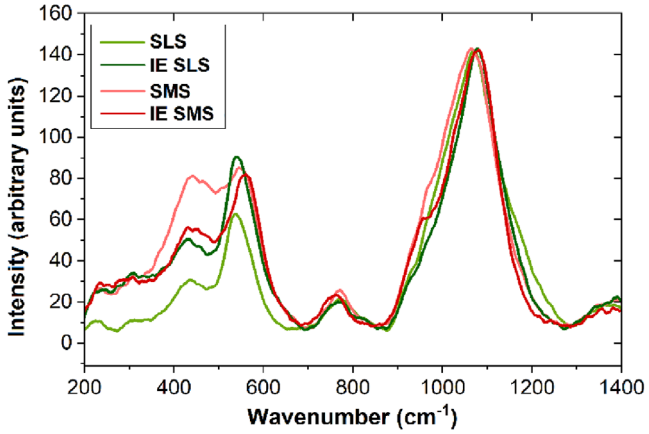

FIGURE 5 Micro-Raman spectra recorded on raw and fully tempered (IE) SLS and SMS glass powder samples after baseline subtraction and normalization.

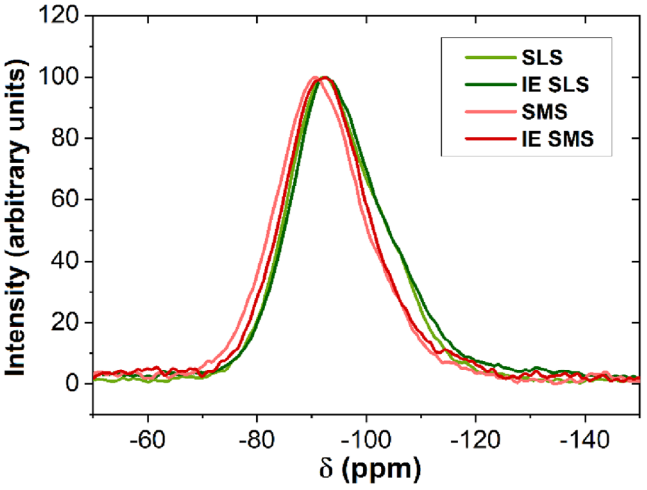

FIGURE 6 ^{29}Si NMR spectra recorded on raw and ion-exchanged (IE) SMS and SLS glass powders.

member siloxane rings and smaller rings; the former contributing to the low frequency tail, the latter displaying signals at higher wavenumber. This region is very sensitive to the variation of cation size and charge, because they modify the Si–O–Si angle and, therefore, the bending mode of SiO_4 tetrahedra[9];

(ii) The intermediate region (MFR, 700–850 cm^{-1}), correlated both with Q^0 units[22] and with bending vibrations of Si–O–Si bridges[20,21];

(iii) The high frequency region (HFR, 850–1300 cm^{-1}) that corresponds to the Si–O stretching vibrations in tetrahedral SiO_4 units differently connected to each other or to other atoms; the peak positions generally accepted are 1120–1190 cm^{-1} for Q^4 units, 1100–1050 cm^{-1} for Q^3, 1000–950 cm^{-1} for Q^2, 900–960 cm^{-1} for Q^1 and 800–850 cm^{-1} for Q^0.[20,22–25]

The spectra of the two glasses show clear differences in both LFR and HFR. In the former, the intensity of the peak at about 450 cm^{-1} as well as of the low wavenumber tail is significantly lower in SLS glass than in SMS one; the SLS glass component at about 550 cm^{-1} is also downshifted with respect to SMS material. The HFR band of SMS glass is observed at a lower wavenumber with respect to SLS glass and presents a more intense left shoulder. Conversely, SLS glass shows a more intense right shoulder.

For both glasses, the ion exchange process induces relevant changes in peak position and intensity in the LFR; in the HFR, SMS shows a small blue shift of the band with the reduction in intensity of the left shoulder; both glasses show a reduction of the band linewidth.

Fitting of the spectra, which was performed by considering all the recognized bands identified as Gaussian functions, is reported in Figure S2 and Table S2. For the sake of clarity, an example is reported in Table 3 corresponding to the IE SMS glass. In detail, the LFR was fitted with five components (labeled as A^1–A^5, Table S3), the MFR with one component (labeled as Q^0), and the HFR with four components (labeled as Q^1–Q^4, Table S3). The profile fitting data (Table S2) can be used to calculate the Raman polymerization index, $RPI = \sum \text{Area}(A^n) / \sum \text{Area}(Q^n)$ (Table 3), namely the ratio between the area of LFR and HFR regions, and it can be used to evaluate the degree of connectivity, which depends on the amount of SiO_2 and modifiers like Na_2O.[10]

According to the work of Grund Bäck et al.,[21] the area of the different Q^n components allows for calculating the ratio $I(Q^3)/I(Q^2+Q^4)$, which is an index of the network variation as a consequence of the exchange of cations with different field strengths.

The parameters reported in Table 3 remark the differences between the two glasses, with lower RPI and less numerous Q^3 units for the SLS glass with respect to the SMS one. The ion exchange process largely increases RPI for soda lime silicate glass, while no effect is shown in the other one; at the same time, the relative amount of Q^3 units increases in both glasses.

Finally, Table S2 confirms the qualitative observation about band shifts reported above. For example, in SMS glass, the LFR components are generally shifted to higher wavenumbers (+10 cm^{-1}) compared with SLS glass, whereas the Q^n bands (HFR) appear at lower wavenumbers (10–20 cm^{-1}), likely due to the presence of Al in the tetrahedral network.[26] After ion exchange, such differences are mostly retained for both glasses, except for the Q^3 band, which shows an opposite shift.

^{29}Si MAS NMR analyses were also run on the four glass powders (Figure 6). It is well known that, as for Raman, the second nearest neighbor of Si influences the chemical shift of the Q units; therefore, it is theoretically possible

TABLE 3 Raman polymerization index (RPI) and $I(Q^3)/I(Q^2 + Q^4)$ values calculated from Raman profile fitting results; an exemplary Raman spectrum profile fitting with the identified band labels is reported on the right.

	RPI	$I(Q^3)/I(Q^2 + Q^4)$
SLS glass	0.34	1.2
IE SLS glass	0.85	2.0
SMS glass	0.79	2.1
IE SMS glass	0.76	2.9

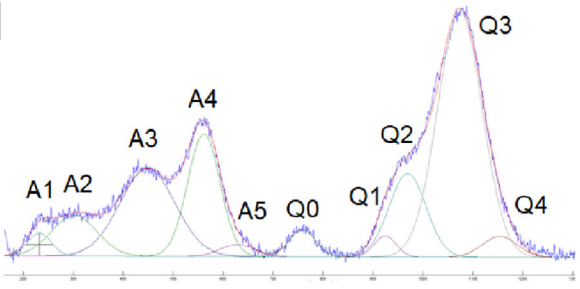

to distinguish both the Q^n units and the nature of the second nearest neighbor atom. Actually, variations of the glass structure induce a change in the chemical shift (δ) that becomes increasingly negative as the number of BO increases, owing to the higher degree of electronic shielding of the central Si atom. Accordingly, Q^4 bands generally fall in the range −102 to −116 ppm, Q^3 between −88 and −101 ppm, and so on. The chemical shift is also influenced by the variation of Si–O bond length and Si–O–Si bridging angles, as well as changes of second and third neighbor atoms, leading to significantly broader spectra.[27,28]

In the present case, the spectra of both raw and ion-exchanged glasses show a single broad silicon resonance centered at about −91 ppm due to the structural Q^n units (Figure 6). The peak maximum is downfield shifted (i.e., at higher δ) with respect to the range of values for pure silica tetrahedra, indicating that most of the Si atoms are bonded to nonbridging oxygens due to the presence of network modifier cations.[27]

Moreover, it is possible to notice a slight downfield shift of the SMS glass peak with respect to the SLS one, which should reflect the relative amount of network formers and modifiers other than Si. The ion exchange process, which does not modify the peak position for SLS glass, induces a visible up-field shift for tempered SMS one, this being explainable with an average bond angle increase and a reduced bond length.[29,30]

The resonances are characterized by an asymmetric line-shape, which indicates the presence of different components due to inequivalent silicon sites, as expected. The Q resonance is composed of Q^4 units with four bridging oxygens, Q^3 and Q^2 units with one or two nonbridging oxygens. Jones et al.[31] found that the number of Q^n components is related to the concentration of M^{n+} cations in the silica network. If $25 < M^{n+} < 40$, as in the present case, Q^2, Q^3, and Q^4 units should be considered. Accordingly, the profile fitting of ^{29}Si spectra was performed by using three components, well reproduced by Gaussian functions (Figure S3),[32] and the results are reported in Table S4.

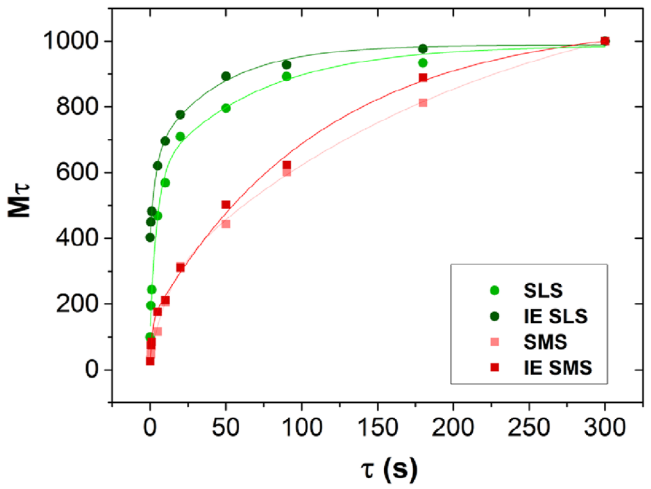

FIGURE 7 *Magnetization recovery*, M_τ, trend for the four glass powders: fitting lines (Equation 2) are also shown.

Soda lime silicate glass shows an almost negligible amount of Q^2, a larger quantity of Q^4 with respect to soda magnesia silicate one, and narrower linewidths (LW) for Q^2 and Q^3 units. For both ion-exchanged glasses, the Q^4 units have larger LW than in the corresponding raw material, whereas Q^3 LW does not change, and Q^2 LW reduces. Moreover, the ion exchange process on SMS glass causes a detectable up-field shift ($\Delta\delta = -2$ ppm) of the Q^3 units (Table S4).

As anticipated before, ^{29}Si T_1 spin-lattice relaxation, which is sensitive to the site symmetry, was studied with the attempt to describe the local order of the silicate network and the possible presence of glass phase separation.[7] Figure 7 shows the magnetization recovery (M_τ) curves as a function of the repetition time (τ) for the whole Q signal. The sum of the Q^n components is considered, encompassing the entire Q signal. Therefore, the observed trend reflects the overall behavior of the glass as a whole, although it results from the contributions of the individual components.

Data points in Figure 7 are fitted with double exponential curves characterized by slow and fast relaxing

components (Equation 2), which indicate the presence of at least two different molecular domains. The results of the fitting analysis are reported in Table S5.

The data for raw and tempered glasses are perfectly fitted with a double exponential with a dominant long relaxing component. Soda lime silicate and soda magnesia silicate glasses are characterized by different internal relaxation phenomena, as suggested by the very different T_1 values. Interestingly, the ion exchange process produces a shortening of the relaxation times in both glasses.

4 | DISCUSSION

The two glasses considered in the present work show a very different behavior when subjected to chemical tempering, the SMS material appearing prone to being reinforced by ion exchange in potassium nitrate. Surface compression and, especially, depth of layer generated in soda magnesia silicate glass are higher than the values obtained in soda lime silicate glass; for example, at 450°C, DOL in soda magnesia silicate glass is almost twice the value measured in soda lime silicate glass. The advantageous effect on the mechanical strength and surface damage resistance appears clear. As reported in several previous works, for both glasses, the surface compression decreases with the ion exchange temperature, this being correlated to relaxation phenomena, which become more intense at temperatures closer to the glass transition range: as shown in Figure 1, the reduction appears more evident in SMS glass.

The mechanical features (CS and DOL) are clearly associated with chemical aspects more connected to the ion exchange process. The depth of layer (Figure 1) must be compared with the potassium penetration depth (Figure 3A). As explained in previous works, there is not a one-to-one correspondence between potassium penetration and the depth of the compressive layer, due to relaxation/reorganization phenomena occurring in the glass structure upon ion exchange and to elastic equilibrium which must be guaranteed across the entire thickness of the glass; nevertheless, one can clearly observe a similar trend in Figure 1 and Figure 3A for DOL and the potassium penetration for both materials analyzed in the present study, SMS glass resulting significantly more efficient in terms of depth reached by the potassium atoms and the corresponding depth of compression.

The interdiffusion coefficient (Figure 3B) provides clear evidence of the different ability of the two glasses to undergo ion exchange and corresponding chemical strengthening.

An additional feature that differentiates the two glasses regards the ion exchange efficiency. Figure 2 shows the K/Na molar ratio as measured by EDXS on the external surface of the treated glasses. Such a ratio increases both with temperature and ion exchange duration; it is worth noting that the K/Na ratio in the bare materials is equal to 0.05 for SLS and 0.01 for SMS glass, i.e. much smaller than the values shown in Figure 2. After the most intensive treatment used in the present work (16 h at 475°C), the K/Na molar ratio is 96.4 and 175.4 for SLS and SMS glass, respectively. The data in Figure 2 clearly represent the concentration in a thin surface layer and therefore can be affected by the electrons' penetration used in the SEM and by the concentration profile of sodium and potassium, the former increasing, the latter decreasing with depth. Therefore, the data in Figure 2 do not represent exactly the surface concentration but can give a very good indication of the surface K/Na molar load evolution with time and temperature. As a matter of fact, the electrons at 20 kV penetrate about 1–2 μm in the glass before interacting with the atoms and activating X-ray emission,[33] making the slope of the concentration profiles important. As said, all profiles could be fitted by an erfc function (Equation 1); if, as an example, profiles with identical depth are considered for the two glasses, for example, 425°C/4 h for SMS and 450°C/16 h for SLS (depth ≈ 30 μm, Figure 3A), although the slope is clearly identical, very different K/Na molar ratio values are measured, 16.9 for SMS and 89.2 for SLS, this confirming the validity of the results in Figure 2 as an efficiency indication of the ion exchange process. Soda magnesia silicate glass shows a greater exchange rate, especially for longer treatments. In any case, as reported also in previous works,[6,34] the sodium/potassium exchange is never totally complete, not even at relatively high temperatures and after long treatment. In other words, a certain amount of sodium always remains unexchanged; even upon the most intensive ion exchange process (16 h at 475°C), the surface concentration of sodium oxide is equal to 0.14 mol% and 0.08 mol% in SLS and SMS glass, respectively. The overall interdiffusion process is clearly different in the two materials, soda magnesia silicate glass being characterized by a greater interdiffusion coefficient (Figure 3B). It is interesting to observe that the activation energy for diffusion is substantially identical for the two glasses, thus pointing out identical mechanisms ruling the atomic movement.

It is of a certain interest to understand the reasons for the very different behavior of the two glasses upon ion exchange in potassium nitrate. The different chemical composition and the corresponding glass structure should be accounted for.

SMS glass contains a larger amount of sodium oxide with respect to SLS one, as reported in Table 1 (14.7 mol% vs. 12.6 mol%). According to previous works, increasing the sodium content in silicate glasses has a positive effect on its diffusion[35,36]: in general, the diffusion coefficient

increases (and, correspondingly, the activation energy for diffusion decreases) by increasing the alkali content in silicate glasses. Unfortunately, the limited available data do not allow for a precise quantification of the effect of the different sodium loads in the glasses considered in the present work on the interdiffusion coefficient evaluated from the concentration profiles. Moreover, it is well known that the presence of divalent or trivalent ions in the glass can significantly influence the alkaline ions interdiffusion phenomenon. Finally, mixed alkali effects, which decrease the ionic mobility, may also occur.[2,35] In the glasses considered here, the difference in terms of sodium content is, anyhow, not so relevant. In terms of atomic concentration, it is about 9% in soda lime silicate glass and 10% in soda magnesia silicate glass. In other words, it seems unlikely that a difference of about 10% in sodium concentration alone could account for an interdiffusion coefficient variation exceeding 40-−50%.

In a previous, very extensive work by Varshneya,[3] among the various means for achieving an increased rate of ion exchange in silicate glass, the author lists, as a final possibility, the addition of small quantities of MgO in the composition. This statement arose from the results published by Sinton et al.,[37] which indicated an increased depth of exchange (and greater interdiffusion coefficient) with larger K_2O and Na_2O content, lower total alkaline earth concentration, lower CaO/MgO ratio, and MgO substituting CaO in the glass. Also, in this case, the comparison of the results by Sinton et al.[37] with those obtained in the present study is challenging due to the influence of multiple compositional factors across the different glasses. In addition, the conclusions drawn by Sinton et al.[37] are affected by considerable uncertainty, the experimental findings reported in the paper being quite scattered. In any case, it is agreeable that a larger alkaline oxide content in the glass is beneficial to promote deeper ion exchange. The same applies to MgO substituting for CaO, as observed in the SMS glass examined here. Sinton et al.[37] reported that "*the replacement of MgO for CaO results in a more open structure, thus decreasing the activation energy required for diffusion*".

Based on the aspects discussed above, undoubtedly, the glass structure must have a prominent role in the ion exchange efficiency, influencing potassium penetration depth, interdiffusion coefficient, and development of deep residual compressive stresses.

The attempt to clarify the role of glass structure was carried out with the use of different spectroscopy techniques, namely, FTIR, Raman, and solid-state NMR. They were also used to obtain quantitative information, since Raman spectroscopy allows the evaluation of both short-range order and medium-range order structural Q^n units present in the glass,[38] and ^{29}Si MAS NMR spectroscopy, which was widely and successfully applied on a variety of silicate systems,[39–42] to provide a measure of the different Q^n unit fractions.

The NMR relaxation study, which provides an average view of the entire material, points out that both SLS and SMS glasses exhibit slow and fast spin-lattice relaxation components (Table S5). This indicates the presence of two distinct molecular domains, in agreement with the modified random network model proposed by Greaves[43,44] where pure Q^4-rich domains are interleaved with modifier-rich channels (Q^n with $n < 4$). In addition, the spin-lattice relaxation time (T_1) values suggest significant differences in the internal reorganization processes, with soda magnesia silicate glass exhibiting greater structural homogeneity. According to Malfait,[45] the higher T_1 values found for SMS glass likely indicate a network with narrower bond angles compared with SLS glass.

The ion exchange process leads to a reduction of the spin-lattice relaxation time in both glasses. This effect is more pronounced in SMS glass, in line with its greater ion exchange ability, which very likely induces a rearrangement of the tetrahedra to accommodate larger potassium cations.

Furthermore, FT-IR spectra (Figure 4) point out structural differences between the two raw glasses, SMS being characterized on average by smaller siloxane angles. This is further confirmed by ^{29}Si NMR (Table S4), which reveals the downfield chemical shift of the center band in raw SMS glass (Figure 6) with respect to SLS. This phenomenon is certainly related to the amount of different network formers and modifiers, which can affect the bond angles among tetrahedra. As a matter of fact, it is expected that the presence of different cations influences both average Si–O bond length ($\langle r_{Si-O} \rangle$) and Si–O–Si angle ($\theta_{Si-O-Si}$), following the generally accepted rules that the chemical shift (δ) moves downfield as $\langle r_{Si-O} \rangle$ increases and upfield if $\theta_{Si-O-Si}$ increases.[30] Moreover, it was proven that for each Q^n (n = 4, 3, 2, 1) species, the chemical shifts increase linearly with the alkali content, thus indicating that ^{29}Si nuclei are less shielded.[32]

If the rules stated by Dawson are considered, the downfield chemical shift shown by the SMS glass band with respect to SLS can be associated with several reasons. It resembles the higher amount of Al atoms that substitute for Si in the tetrahedral network, forming Si–O–Al linkages. According to the composition of the glasses, Si–O species are the most probable Al neighbors,[27] and ^{27}Al MAS measurements performed on SMS glass proved that Al is in tetrahedral coordination (Figure S4). In addition, the larger amount of Mg^{2+} (with a lower ionic radius and higher ionic potential Z/r, where Z = valence and r = ionic radius) with respect to Ca^{2+} should favor smaller angles for SMS glass, contributing to the downfield shift.,[29,30] The

Mg^{2+} ability to play a network former role, thus connecting to other network formers via bridging oxygen and forming shorter and stronger bonds with NBO, should also be considered.[46,47]

Therefore, if one considers the initial composition of the two glasses, the insertion of potassium with a larger ionic radius and coordination ability upon ion exchange leads to a greater rearrangement in terms of bond lengths and angles for SMS glass, thus causing an upfield shift of the corresponding ^{29}Si center-band and wider linewidth of the Q^4 component for both glasses.

According to Maekawa et al.,[32] the linewidth of the components is directly correlated to the ionic potential (*Z/r*) of the cations. Following Stebbins[48] for diffusion phenomena carried out below the glass transition temperature, the number of NBO and BO is fixed; when a cation is replaced by a larger one, like Na by K, the coordination number increases, and this means that larger cations involve in coordination also some BO. Such structural evolution modifies the bond angles of the Q^4 species, increasing the disorder and, consequently, the linewidth (LW) signal; this could also explain the observed blue shift of BO components in the FTIR spectrum of SMS glass (Table S1).

The analysis of the Raman spectra further confirms the above findings. The ratio among the Q^n units differentiates the two glasses, with SMS glass exhibiting a higher proportion of Q^3 units and a lower presence of Q^2 and Q^4 units. This is likely due to the greater abundance of network formers, such as Al and possibly Mg. In addition, the presence of aluminum induces the band shifts (Table S2). The Si–O–Si bending vibration bands (A^n in the LFR, Table S2) for soda magnesia silicate glass are generally located at higher wavenumbers (+10 cm^{-1}) with respect to soda lime silicate glass, consistent with a reduction of the Si–O–Si bond angle.[49] Furthermore, the Q^n bands appear at lower wavenumbers (10–20 cm^{-1}), which can be attributed to the contribution of Si–O–Al bonds within the tetrahedral network.

The ion exchange treatment has a similar impact on both glasses with an increase of the Q^3 unit at the expense of the Q^4, probably because of the replacement of higher field strength cations (cation field strength = Z/r^2, where Z = valence and r = cation radius in angstrom) by lower field strength K^+ ions, as found by Grund Bäck et al.[21]

It is known that the results obtained from the Raman spectra could be affected by some errors, such as the oscillation strength of the different absorbing units and the effect of background correction.[38] Moreover, the variability of the Q^n parameters (wavenumber and components) among several authors reduces the reliability of the conclusions. For this reason, some authors agree with the choice to evaluate just the RPI.[10] In fact, RPI, defined as the ratio between LFR and HFR areas, provides insights into the degree of connectivity in silicate glasses,[10] where a higher index indicates greater connectivity. As shown in Figure 4 and Table 3, RPI differs significantly between the two glasses, the LFR area being considerably smaller in the SLS material.

The difference in this region reflects the distinct cation compositions of the two glasses. In fact, the total LFR intensity, as well as the intensity of its various components, can be related to several factors, such as the amount of SiO_2 and Na_2O, as well as the (MgO+CaO)/SiO_2 and MgO/CaO ratios.[10] In particular, the spectral intensity in the region below 450 cm^{-1}, which includes the signals from large siloxane rings, is typically reduced by increasing the amount of alkaline earth elements, but it increases with Mg content.[10]

SLS and SMS glasses have the same (MgO+CaO)/SiO_2 ratio, but the MgO/CaO one is significantly higher in SMS, which also has a slightly lower SiO_2 content but a quite similar Na_2O concentration. These factors can explain both the larger intensity of signals in the range 250–480 cm^{-1} and the blue shift of the component at 550 cm^{-1} in SMS glass.

The ion exchange process leads to a significant increase in the RPI for soda lime silicate glass, due to the growth of the LFR area, particularly the components associated with large rings. Conversely, RPI in soda magnesia silicate glass is only slightly decreased, mainly due to the reduction in the low-wavenumber components.

These results suggest that the SMS glass network, characterized by a higher proportion of 5–6-member and larger rings, is more amenable to the substitution of sodium with potassium, thus explaining its greater interdiffusion coefficient. While this substitution leads to notable changes in the local environment of Si units, as evidenced by NMR, it does not appear to require substantial alterations in the medium-range order. This is consistent with the observation that the activation energy for diffusion is very similar, pointing out that the atomic movement is governed by the same mechanisms in both glasses.

5 | CONCLUSION

The two materials considered in the present work, a soda lime silicate and a soda magnesia silicate glass, both produced by the float process and exhibiting very similar thermo-mechanical properties, revealed a very different behavior when subjected to chemical strengthening through the ion exchange process in potassium nitrate. Specifically, soda magnesia silicate glass shows a much higher interdiffusion coefficient, which leads to deeper potassium penetration and, consequently, a higher residual compression for the same treatment duration.

This performance can be attributed to the different glass structure, with the soda-magnesia silicate glass containing a larger number of five- or more-membered rings, due to the higher concentration of glass formers (SiO_2, Al_2O_3, and, very likely, MgO) in its composition.

The obtained results suggest a pathway for producing glasses with enhanced chemical strengthening performances, starting from the composition to develop glass structures more suited to undergo ion exchange.

ACKNOWLEDGMENTS

The authors acknowledge Miss Albina Abdurakhmanova, Miss Alexia Conci, and Mr Alessandro Rizzi (University of Trento) for preparing the glass samples, performing the EDXS analyses, and the surface compression/case depth measurements. They also acknowledge Dr. Alessandro Chiasera and Dr. Suda Maria Lis Scaria (IFN-CNR, Trento) for the refractive index measurement, the University of Trento for the financial support, and Pilkington Italia Spa—NSG at San Salvo (CH, Italy) for providing the soda magnesia silicate glass.

Open access publishing facilitated by Universita degli Studi di Trento, as part of the Wiley - CRUI-CARE agreement.

ORCID

Vincenzo M. Sglavo https://orcid.org/0000-0001-9133-7204

REFERENCES

1. Acloque P, Tochon J. Measurement of mechanical resistance of glass after reinforcement. In Colloquium on Mechanical Strength of Glass and Ways of Improving It, Charleroi, Belgium: Union Scientifique Continentale du Verre, 1961, p. 687–704.
2. Varshneya ArunK, Mauro JC. Fundamentals of Inorganic Glasses. Elsevier; 2019. https://doi.org/10.1016/C2017-0-04281-7
3. Varshneya AK. Chemical strengthening of glass: lessons learned and yet to be learned. Int J Appl Glass Sci. 2010;1(2):131–42, https://doi.org/10.1111/j.2041-1294.2010.00010.x
4. Varshneya AK. The physics of chemical strengthening of glass: room for a new view. J Non-Crystal Solid. 2010; 2289–94. https://doi.org/10.1016/j.jnoncrysol.2010.05.010
5. Mazzoldi P, Carturan S, Quaranta A, Sada C, Sglavo VM. Ion exchange process: history, evolution and applications. La Rivista del Nuovo Cimento. 2013;36(9):397–460, https://doi.org/10.1393/ncr/i2013-10092-1
6. Sglavo VM. Chemical strengthening of soda lime silicate float glass: effect of small differences in the KNO_3 bath. Int J Appl Glass Sci. 2015;6(1): https://doi.org/10.1111/ijag.12101
7. Mortuza MG, Dupree R, Holland D. 29Si T1 relaxation in alkali silicate glasses: a method for detecting glass-in-glass phase separation. J Non Cryst Solids. 2001;281(1–3):108–16, https://doi.org/10.1016/S0022-3093(00)00440-3
8. Massiot D, Fayon F, Capron M, King I, Calvé SL, Alonso B, et al. "Modelling one- and two-dimensional solid-state NMR spectra." Magnetic Resonance Chem. 2002;40(1):70–76, https://doi.org/10.1002/mrc.984
9. Colomban P, Tournie A, Bellot-Gurlet L. Raman identification of glassy silicates used in ceramics, glass and jewellery: a tentative differentiation guide. J Raman Spectrosc. 2006;37(8):841–52, https://doi.org/10.1002/jrs.1515
10. Kilinc E, Hand RJ. Mechanical properties of soda–lime–silica glasses with varying alkaline earth contents. J Non Cryst Solids. 2015;429:190–7, https://doi.org/10.1016/j.jnoncrysol.2015.08.013
11. Ragoen C, Sen S, Lambricht T, Godet S. Effect of Al 2 O 3 content on the mechanical and interdiffusional properties of ion-exchanged Na-aluminosilicate glasses. J Non Cryst Solids. 2017;458:129–36, https://doi.org/10.1016/j.jnoncrysol.2016.12.019
12. Karlsson S, Mathew R, Ali S, Paemurru M, Anton J, Stevensson B, et al. Mechanical, thermal, and structural investigations of chemically strengthened Na2O–CaO–Al2O3–SiO2 glasses. Front Mater. 2022;9, https://doi.org/10.3389/fmats.2022.953759
13. Ingram MD, Wu M-H, Coats A, Kamitsos EI, Varsamis C-PE, Garcia N, et al. "Evidence from infrared spectroscopy of structural relaxation during field assisted and chemically driven ion exchange in soda-lime-silica glasses." Phys Chem Glass. 2005;46(2):84–9.
14. Lee Y. IR reflection spectroscopy of a soda-lime glass surface during ion-exchange. J Non Cryst Solids. 1997;222(1–2):125–30, https://doi.org/10.1016/S0022-3093(97)00391-8
15. Sharaf NA, Condrate RA, Ahmed AA. FTIR spectral/structural investigation of the ion exchange/thermal treatment of silver ions into a silicate glass. Mater Lett. 1991;11(3–4):115–8, https://doi.org/10.1016/0167-577X(91)90097-P
16. Taylor WR. Application of infrared spectroscopy to studies of silicate glass structure: examples from the melilite glasses and the systems Na_2O-SiO_2 and Na_2O-Al_2O_3-SiO_2. J Earth Syst Sci. 1990;99(1):99–117, https://doi.org/10.1007/BF02871899
17. Luo J, Zhou Y, Pantano CG, Kim SH. Correlation between IR peak position and bond parameter of silica glass: molecular dynamics study on fictive temperature (cooling rate) effect. J Am Ceram Soc. 2018;101(12):5419–27, https://doi.org/10.1111/jace.15858
18. Grill A, Neumayer DA. Structure of low dielectric constant to extreme low dielectric constant SiCOH films: Fourier transform infrared spectroscopy characterization. J Appl Phys. 2003;94(10):6697–707, https://doi.org/10.1063/1.1618358
19. Galeener FL, Geissberger AE. Vibrational dynamics in 30Si-substituted vitreous SiO_2. Phys Rev B. 1983;27(10:)6199–204, https://doi.org/10.1103/PhysRevB.27.6199
20. McMillan P. Structural studies of silicate glasses and melts-applications and limitations of Raman spectroscopy. Am Mineralogist. 1984;69(69):622–44,
21. Bäck LGrund, Ali S, Karlsson S, Möncke D, Kamitsos EI, Jonson B. Mixed alkali/alkaline earth-silicate glasses: physical properties and structure by vibrational spectroscopy. Int J Appl Glass Sci. 2019;10(3):349–62, https://doi.org/10.1111/ijag.13101
22. Colomban P. Polymerization degree and Raman identification of ancient glasses used for jewelry, ceramic enamels and mosaics. J Non Cryst Solids. 2003;323(1–3):180–7, https://doi.org/10.1016/S0022-3093(03)00303-X
23. Lenoir M, Grandjean A, Poissonnet S, Neuville DR. Quantitation of sulfate solubility in borosilicate glasses using Raman

spectroscopy. J Non Cryst Solids. 2009;355(28–30):1468–73, https://doi.org/10.1016/j.jnoncrysol.2009.05.015
24. Fukumi K, Hayakawa J, Komiyama T. Intensity of raman band in silicate glasses. J Non Cryst Solids. 1990;119(3):297–302, https://doi.org/10.1016/0022-3093(90)90302-3
25. Colomban P, Tournie A, Bellot-Gurlet L. Raman identification of glassy silicates used in ceramics, glass and jewellery: a tentative differentiation guide. J Raman Spectrosc. 2006;37(8):841–52, https://doi.org/10.1002/jrs.1515
26. Bechgaard TK, Scannell G, Huang L, Youngman RE, Mauro JC, Smedskjaer MM. Structure of MgO/CaO sodium aluminosilicate glasses: Raman spectroscopy study. J Non Cryst Solids. 2017;470:145–51, https://doi.org/10.1016/j.jnoncrysol.2017.05.014
27. Prasad S, Clark TM, Sefzik TH, Kwak H-T, Gan Z, Grandinetti PJ. Solid-state multinuclear magnetic resonance investigation of Pyrex®. J Non Cryst Solids. 2006;352(26–27):2834–40, https://doi.org/10.1016/j.jnoncrysol.2006.02.085
28. Stebbins JF. Anionic speciation in sodium and potassium silicate glasses near the metasilicate ($[Na,K]_2SiO_3$) composition: 29Si, 17O, and 23Na MAS NMR. J Non-Crystal Solids: X. 2020;6:100049, https://doi.org/10.1016/j.nocx.2020.100049
29. Mauri F, Pasquarello A, Pfrommer BG, Yoon Y-G, Louie SG. Si-O-Si bond-angle distribution in vitreous silica from first-principles 29 Si NMR analysis. Phys Rev B. 2000;62(8):R4786–9, https://doi.org/10.1103/PhysRevB.62.R4786
30. Dawson DM, Moran RF, Ashbrook SE. An NMR crystallographic investigation of the relationships between the crystal structure and ^{29} Si isotropic chemical shift in silica zeolites. J Phys Chem C. 2017;121(28):15198–210, https://doi.org/10.1021/acs.jpcc.7b03730
31. Jones AR, Winter R, Greaves GN, Smith IH. MAS NMR study of soda-lime–silicate glasses with variable degree of polymerisation. J Non Cryst Solids. 2001;293–295:87–92, https://doi.org/10.1016/S0022-3093(01)00656-1
32. Maekawa H, Maekawa T, Kawamura K, Yokokawa T. The structural groups of alkali silicate glasses determined from 29Si MAS-NMR. J Non Cryst Solids. 1991;127(1):53–64, https://doi.org/10.1016/0022-3093(91)90400-Z
33. Zhou W, Apkarian R, Wang ZL, Joy D. Fundamentals of scanning electron microscopy (SEM). In: Scanning Microscopy for Nanotechnology, New York, NY: Springer New York; 2006, p. 1–40. https://doi.org/10.1007/978-0-387-39620-0_1
34. Sglavo VM. Influence of bath composition on chemical strengthening process of commercial silicate glass. In: *Materials Science and Technology Conference and Exhibition*, *MS&T 2012*; 2012.
35. Doremus RH. Glass science, 2nd ed. Wiley; 1994.
36. Frischat GH. Ionic diffusion in oxide glasses;8. Trans Tech Publications; 1985. https://doi.org/10.4028/www.scientific.net/RC.8
37. Sinton CW, LaCourse WC, O'Connell MJ. Variations in K+–Na+ ion exchange depth in commercial and experimental float glass compositions. Mater Res Bull. 1999;34(14–15):2351–59, https://doi.org/10.1016/S0025-5408(00)00163-X
38. Parkinson BG, Holland D, Smith ME, Larson C, Doerr J, Affatigato M, et al. Quantitative measurement of Q3 species in silicate and borosilicate glasses using Raman spectroscopy. J Non Cryst Solids. 2008;354(17):1936–42, https://doi.org/10.1016/j.jnoncrysol.2007.06.105
39. Pedone A. Recent advances in solid-state NMR computational spectroscopy: the case of alumino-silicate glasses. Int J Quantum Chem. 2016;116(21:1520–31, https://doi.org/10.1002/qua.25134
40. Curtis NJ, Gascooke JR, Johnston MR, Pring A. 29Si Solid-State NMR analysis of Opal-AG, Opal-AN and Opal-CT: single pulse spectroscopy and spin-lattice T1 relaxometry. Minerals. 2022;12(3):323, https://doi.org/10.3390/min12030323
41. Eckert H. Spying with spins on messy materials: 60 years of glass structure elucidation by <scp>NMR</scp>spectroscopy. Int J Appl Glass Sci. 2018;9(2):167–87, https://doi.org/10.1111/ijag.12333
42. Youngman R. NMR spectroscopy in glass science: a review of the elements. Materials. 2018;11(4):476, https://doi.org/10.3390/ma11040476
43. Greaves GN. EXAFS and the structure of glass. J Non Cryst Solids. 1985;71(1–3):203–17, https://doi.org/10.1016/0022-3093(85)90289-3
44. Greaves GN. EXAFS, glass structure and diffusion. Philosophical Magazine B. 1989;60(6):793–800, https://doi.org/10.1080/13642818908209743
45. Malfait WJ, Halter WE, Verel R. 29Si NMR spectroscopy of silica glass: T1 relaxation and constraints on the Si–O–Si bond angle distribution. Chem Geol. 2008;256(3–4):269–77, https://doi.org/10.1016/j.chemgeo.2008.06.048
46. Mauri F, Pasquarello A, Pfrommer BG, Yoon Y-G, Louie SG. Si-O-Si bond-angle distribution in vitreous silica from first-principles 29 Si NMR analysis. Phys Rev B. 2000;62(8):R4786–9, https://doi.org/10.1103/PhysRevB.62.R4786
47. Watts SJ, Hill RG, O'Donnell MD, Law RV. Influence of magnesia on the structure and properties of bioactive glasses. J Non Cryst Solids. 2010;356(9–10):517–24, https://doi.org/10.1016/j.jnoncrysol.2009.04.074
48. Stebbins JF. Cation sites in mixed-alkali oxide glasses: correlations of NMR chemical shift data with site size and bond distance. Solid State Ion. 1998;112(1–2):137–41, https://doi.org/10.1016/S0167-2738(98)00224-0
49. Hruška B, Gavenda T, Vašíček F, Svoboda R. Raman spectroscopy study of glass corrosion. Vib Spectrosc. 2020;109:103096, https://doi.org/10.1016/j.vibspec.2020.103096

SUPPORTING INFORMATION

Additional supporting information can be found online in the Supporting Information section at the end of this article.

How to cite this article: Sglavo VM, Bettotti P, Callone E, Dirè S. Chemical strengthening of float glasses: Effect of composition and structure. J Am Ceram Soc. 2026;109:e70317. https://doi.org/10.1111/jace.70317